Horizon volumes with interpreted constraints

Xinming Wu & Dave Hale
Center for Wave Phenomena, Colorado School of Mines, Golden, CO 80401, USA

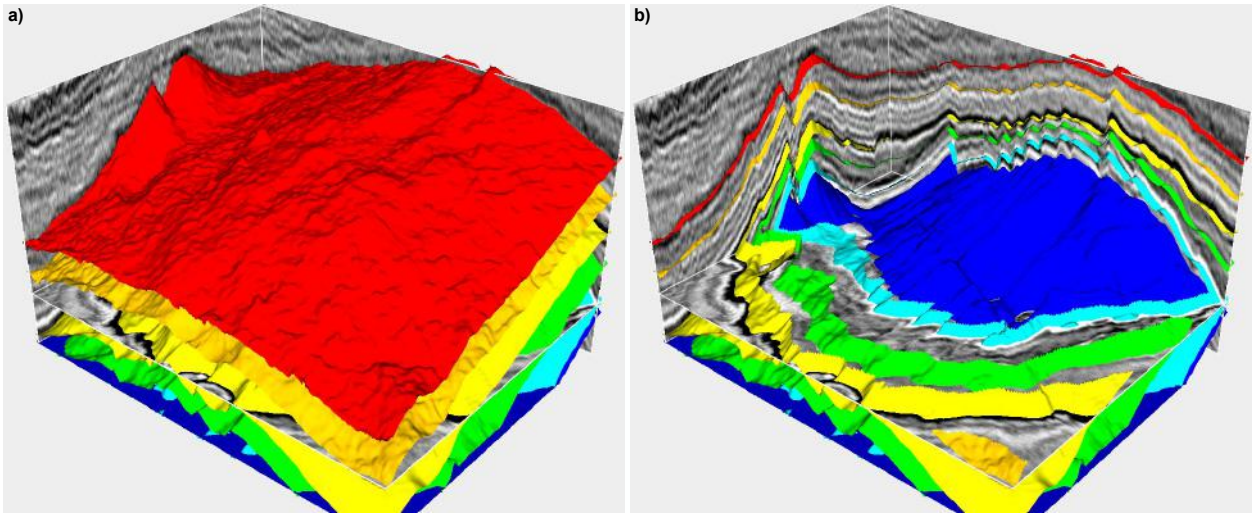

Figure 1. A 3D view of 6 seismic horizons (a) with cut-away views (b) to show more details. These horizons are a small subset of those in a complete horizon volume.

ABSTRACT
We propose two methods for constructing seismic horizons aligned with reflectors in a 3D seismic image. The first method extracts horizons one at a time; the second generates at once an entire volume of horizons. The most significant new aspect of both methods is the ability to specify, perhaps interactively during interpretation, a small number of control points that may be scattered throughout a 3D seismic image. Examples show that control points enable the accurate extraction of horizons from seismic images in which noise, unconformities, and faults are apparent. These points represent constraints that we implement simply as preconditioners in the conjugate gradient method used to construct horizons.

Key words: seismic horizon volume RGT flattening normal vectors

1 INTRODUCTION

In seismic interpretation, by visually tracking or automatically extracting surfaces throughout a 3D seismic image along amplitude peaks or troughs, we are able to identify seismic horizons. These horizons correspond to stratal surfaces which are primary beddings or ancient depositional surfaces that are geologically synchronous (Vail et al., 1977). Color-coding of horizons based on amplitude or other attributes can help reveal ancient depositional environments and geomorphic features (Posamentier et al., 2007). Therefore, extracting horizons from seismic images is a common and important problem for seismic interpretation.

1.1 Horizon volume

Lomask (2010a,b) first presented the concept of a "horizon volume" (Figure 2c), which can be generated from a seismic image (Figure 2a) and used to flatten reflec-

tors (Figure 2d) or to access all horizons at once. A horizon volume $z(x,y,\tau)$ (Figure 2c) contains horizon depth z as a function of relative geologic time (RGT) τ and horizontal spatial coordinates x and y. Therefore, horizontally slicing a horizon volume yields the spatial locations (x, y, and z) of a horizon corresponding to a constant RGT τ.

The concept of an "RGT volume" (Figure 2b), first presented by (Stark, 2005), is closely related to the "horizon volume." An RGT volume $\tau(x,y,z)$ (Figure 2b) contains RGT τ as a function of spatial coordinates x, y and z. The contours of constant τ in an RGT volume correspond to seismic horizons. The only difference between an RGT volume and its corresponding seismic image is that the value of a sample in an RGT volume represents geologic time rather than seismic amplitude (Stark, 2005).

Given an RGT volume $\tau(x,y,z)$ with τ monotonically increasing with its vertical coordinate z, a horizon volume $z(x,y,\tau)$ can be easily obtained via an inverse linear interpolation method, as discussed by Parks (2010). In practice, we use both volumes to conveniently access horizons. An RGT volume, with axes identical to a seismic image, is first used to look up the RGT value τ for a horizon we wish to extract. A horizon volume is then used to directly obtain the spatial coordinates for the horizon by simply horizontally slicing the horizon volume for that τ.

1.2 Previous methods

Methods for obtaining a horizon volume can be generally classified into three categories. The first is stratal slicing (Zeng et al., 1998a,b), which uses several reference horizons to interpolate a set of horizons that form a horizon volume. With a limited number of horizons for control, the interpolated horizon volume can follow large-scale features but usually cannot resolve local features (Lomask, 2013).

The second category of methods uses seismic reflector dips (Lomask et al., 2006; Parks, 2010) or, equivalently, *seismic normal vectors*, computed for every image sample to be perpendicular to seismic reflectors (Luo and Hale, 2012). In these methods, a horizon volume is explicitly (Lomask et al., 2006) or implicitly (Parks, 2010; Luo and Hale, 2012) generated to map a seismic image from the depth-space domain to a flattened image in the RGT-space domain.

The third category is similar to the second one in that these methods flatten an entire 3D seismic image, but without use of dips or normal vectors. Instead, they use an RGT volume generated by unwrapping a corresponding seismic instantaneous phase image (Stark, 2005; Wu and Zhong, 2012a). The last two categories of methods automatically identify all horizons in a seismic image at once. Horizon volumes generated by these methods are more accurate for revealing local features

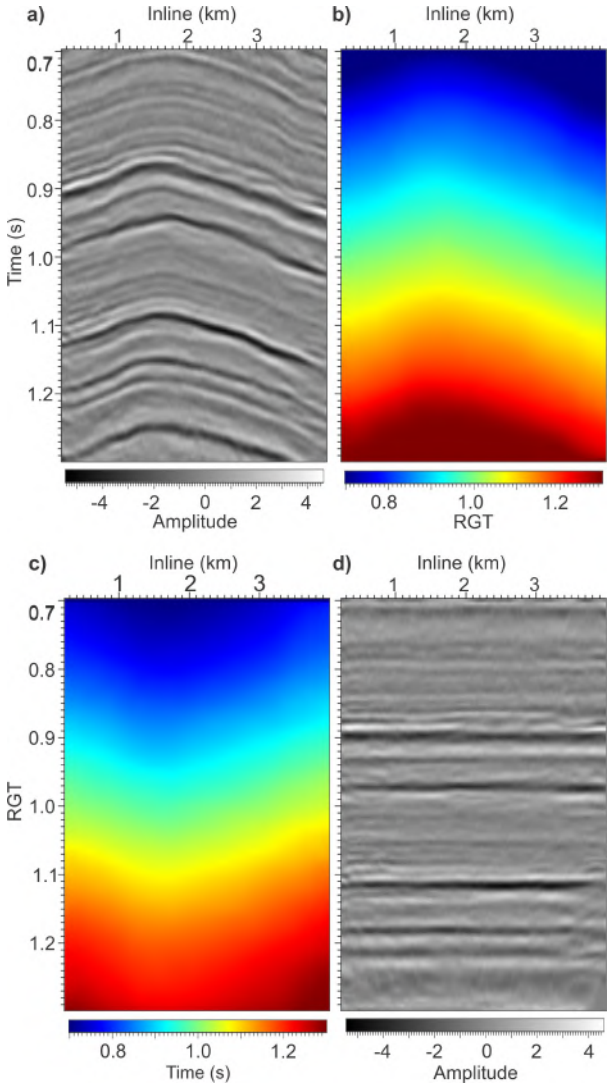

Figure 2. From a seismic image (a), a RGT volume (b) is computed and then converted to a horizon volume (c) that maps the seismic image to a flattened image (d).

than those interpolated from several horizons using the first category of methods.

1.3 This paper

In this paper, we first describe a method for extracting single horizons, one at a time, by using precomputed seismic normal vectors which are normal to seismic reflectors. This method requires at least one control point to indicate the horizon (containing this point) that we want to extract and to initialize a horizontal surface passing through this point. The initial surface is typically inconsistent with the desired horizon, but it is iteratively deformed until vectors normal to the surface are aligned with vectors normal to a reflector in the seis-

mic image. We extend this method to permit additional control points, which enable reliable extraction of a sequence boundary or a horizon complicated by faults or noise.

We then introduce a second method that generates a complete horizon volume constrained by multiple sets of control points. To generate a horizon volume (Figure 2c), we first use seismic normal vectors to compute an RGT volume (Figure 2b), from which a horizon volume is then interpolated. This process is similar to Parks's (2010) method for flattening a seismic image, but we instead derive the method in a simpler way. Furthermore, similar to the way in which we extract a more accurate single horizon using control points, we use multiple sets of control points to generate a more accurate horizon volume from a seismic image complicated by faults or noise. Each set of control points belongs to a single horizon with an unspecified RGT value, and is easily specified in seismic interpretation by simply selecting points that we want to lie on the same horizon. We implement these constraints with simple preconditioners in the conjugate gradient (CG) algorithm we use to compute the RGT and horizon volumes.

2 EXTRACTING A SINGLE HORIZON

To extract or construct a single horizon from a 3D seismic image, one usually first picks a reference point or seed. This seed then grows to a horizon surface by manually or automatically tracking seismic reflectors along seismic amplitude peaks or troughs.

Here, we describe a different method that uses at least one control point to initialize a complete horizontal surface and then updates that surface to conform to seismic normal vectors. We then extend this method to enable use of multiple control points, which improve both the accuracy and efficiency of horizon extraction.

2.1 Horizon extraction without constraints

We first use structure tensors (van Vliet and Verbeek, 1995; Fehmers and Höcker, 2003) to compute, for each image sample, a unit vector $\mathbf{n} = [n_x \ n_y \ n_z]^\top$ that is perpendicular to the seismic reflector at that sample location (Luo and Hale, 2012). We then assume a single-valued horizon surface $z = f(x, y)$ and define the surface implicitly by

$$U(x, y, z) = z - f(x, y). \tag{1}$$

Then unit vectors normal to the surface are

$$\mathbf{n}_s = \frac{\nabla U(x,y,z)}{\|\nabla U(x,y,z)\|} = \alpha \begin{bmatrix} -\frac{\partial f}{\partial x} \\ -\frac{\partial f}{\partial y} \\ 1 \end{bmatrix}, \tag{2}$$

where α is a scale factor that makes $\mathbf{n}_s$ a unit vector.

The seismic horizon we seek is a surface whose normal vectors $\mathbf{n}_s$ equal the seismic normal vectors $\mathbf{n}$ at all positions (x, y, z) on the horizon. However, we initially do not know the positions of the horizon. To solve this problem, we must iteratively update an initial horizontal surface $f^0(x, y)$, by solving

$$\alpha^i \begin{bmatrix} -\frac{\partial f^i}{\partial x} \\ -\frac{\partial f^i}{\partial y} \\ 1 \end{bmatrix} = \begin{bmatrix} n_x^{i-1} \\ n_y^{i-1} \\ n_z^{i-1} \end{bmatrix}. \tag{3}$$

Here, $f^i(x, y)$ is the surface to be updated at the $i-th$ iteration; $n_x^{i-1} = n_x(x, y, f^{i-1}(x, y))$, $n_y^{i-1} = n_y(x, y, f^{i-1}(x, y))$, and $n_z^{i-1} = n_z(x, y, f^{i-1}(x, y))$ are the components of seismic normal vectors at positions on the surface obtained in the $(i-1)-th$ iteration.

To start this iterative process, we initialize a horizontal surface $f^0(x, y)$ (black lines in Figure 3a) passing through a control point (green circle in Figure 3a) that is located on the seismic horizon we want to extract. This initial surface is then iteratively updated to align with the seismic horizon. In each iteration, we eliminate α^i by setting $\alpha^i = n_z^{i-1}$, and then solve the following *inverse-gradient* problem (Farnebäck et al., 2007) to update the surface $f^i(x, y)$:

$$\begin{bmatrix} \frac{\partial f^i}{\partial x} \\ \frac{\partial f^i}{\partial y} \end{bmatrix} = \begin{bmatrix} p^{i-1} \\ q^{i-1} \end{bmatrix}, \tag{4}$$

where $p^{i-1} = -n_x^{i-1}/n_z^{i-1}$ and $q^{i-1} = -n_y^{i-1}/n_z^{i-1}$ are reflector slopes in the x and y directions, respectively. These two equations should be satisfied for every sample on the horizon, but it usually helps to weight these equations by some measure $w(x, y, z)$ of the quality of the estimated reflector slopes. For example, $w(x, y, z)$ can be a measure of local planarity in the seismic image, easily computed from structure tensors (Hale, 2009). Then,

$$w^{i-1} \begin{bmatrix} \frac{\partial f^i}{\partial x} \\ \frac{\partial f^i}{\partial y} \end{bmatrix} = w^{i-1} \begin{bmatrix} p^{i-1} \\ q^{i-1} \end{bmatrix}, \tag{5}$$

where $w^{i-1} = w(x, y, f^{i-1}(x, y))$.

Assuming we have N sampled locations on the horizon surface, we will have $2N$ weighted equations for the N unknowns $f^i(x, y)$. For each iteration, we discretize these equations to obtain the corresponding matrix form

$$\mathbf{WGf} = \mathbf{Wv}, \tag{6}$$

where $\mathbf{W}$ is a $2N \times 2N$ diagonal matrix containing weights $w(x, y, f^{i-1}(x, y))$, $\mathbf{G}$ is a $2N \times N$ sparse matrix obtained by discretizing partial derivatives, $\mathbf{v}$ is a $2N \times 1$ vector containing the seismic reflector slopes p^{i-1} and q^{i-1} on the surface $f^{i-1}(x, y)$ obtained in the previous iteration, and $\mathbf{f}$ is an $N \times 1$ vector containing surface

depths $f^i(x,y)$ we want to find.

Because this inverse gradient problem has more equations than unknowns, we compute its least-squares solution by solving the normal equations

$$(\mathbf{WG})^\top \mathbf{WGf} = (\mathbf{WG})^\top \mathbf{Wv}. \tag{7}$$

To simplify this equation, we let $\mathbf{A} = (\mathbf{WG})^\top \mathbf{WG}$ and $\mathbf{b} = (\mathbf{WG})^\top \mathbf{Wv}$ to obtain

$$\mathbf{Af} = \mathbf{b}. \tag{8}$$

It is convenient that the matrix $\mathbf{A} = \mathbf{G}^\top \mathbf{W}^\top \mathbf{WG}$ is symmetric positive definite (SPD), as this enables use of the CG method to solve this linear system.

2.1.1 Preconditioner

To accelerate the convergence of CG iterations, Harlan (1995) suggests use of a model reparameterization $\mathbf{f} = \mathbf{S}\tilde{\mathbf{f}}$, where $\mathbf{S}$ is a simplification operator designed to create the desired features in the solution $\mathbf{f}$. Applying this technique to the system of equation 8, we first solve a new system

$$\mathbf{S}^\top \mathbf{AS}\tilde{\mathbf{f}} = \mathbf{S}^\top \mathbf{b} \tag{9}$$

for the new unknowns $\tilde{\mathbf{f}}$ and then compute the desired solution $\mathbf{f} = \mathbf{S}\tilde{\mathbf{f}}$. For an appropriate operator $\mathbf{S}$, the CG method applied to the new system of equation 9 converges much faster than for the original system of equation 8.

In effect, this model reparameterization is equivalent to *split preconditioning* (Saad, 1996) with left and right preconditioners $\mathbf{M}_L^{-1} = \mathbf{S}^\top$ and $\mathbf{M}_R^{-1} = \mathbf{S}$. As noted by Saad (1996) and others, this split preconditioning can be implemented with a left preconditioning matrix $\mathbf{M} = \mathbf{M}_L\mathbf{M}_R$ in a preconditioned CG solution of

$$\mathbf{M^{-1}Af} = \mathbf{M^{-1}b}, \tag{10}$$

where $\mathbf{M^{-1}} = \mathbf{SS}^\top$.

Recall that $\mathbf{S}$ is a simplification operator used to facilitate desired features in the solution (Harlan, 1995). Here, we implement $\mathbf{S}$ as a smoothing operator $\mathbf{S} = \mathbf{S}_x\mathbf{S}_y$, where $\mathbf{S}_x$ and $\mathbf{S}_y$ are axis-aligned smoothing filters in the x and y directions, respectively. A horizon surface $\mathbf{f}$ is often smooth, except at faults. Therefore, our $\mathbf{S}_x$ and $\mathbf{S}_y$ are spatially variant smoothing filters (Hale, 2009), with the extent of smoothing controlled by a measure of discontinuity of seismic reflectors. This measure could be planarity (Hale, 2009) or fault likelihood (Hale, 2013). Here we use planarity, computed from structure tensors, to control the extent of smoothing in $\mathbf{S}_x$ and $\mathbf{S}_y$.

Now, for each iteration (equation 5) that updates the surface $f^i(x,y)$, we solve equation 8 using the preconditioned CG method with preconditioner

$$\mathbf{M^{-1}} = \mathbf{S}_x\mathbf{S}_y\mathbf{S}_y^\top\mathbf{S}_x^\top. \tag{11}$$

In this way, we iteratively update the surface $z = f(x,y)$ until its normal vectors $\mathbf{n}_s$ are aligned with the seismic normal vectors $\mathbf{n}(x,y,z=f(x,y))$.

In summary, given an initially horizontal surface (black curves in Figure 3) that is inconsistent with any seismic reflector, our method iteratively reduces the difference between the normal vectors $\mathbf{n}_s$ of the surface and the seismic normal vectors $\mathbf{n}(x,y,f(x,y))$ on the surface to obtain a single seismic horizon surface (blue curves in Figure 3).

2.2 Results without constraints

In Figure 3, using only one control point to indicate which horizon we want to extract, our method updates the initially horizontal surface to the more nearly correct seismic horizon (blue curves in Figure 3) after 9 iterations. The extracted surface is well-aligned with the seismic horizon at conformable areas in the left section of Figure 3a. However, in the sections shown in Figure 3b, this iterative method fails to update the horizon surface to the location of the angular unconformity (green dashed curve in Figure 3b).

Extracting such a sequence boundary or unconformity is an important but difficult problem in seismic interpretation. From structure tensors, we failed to correctly estimate the discontinuous normal vectors at the unconformity and therefore obtained the incorrect horizon surface shown in Figure 3b. In the next section, we will describe a method to correctly extract a sequence boundary using control points.

2.3 Horizon extraction with constraints

Near unconformities, faults, or in areas where an image is noisy, estimated seismic normal vector are not accurate enough to automatically obtain a correct sequence boundary or horizon. Therefore, instead of using a fully automatic method, we might manually interpret the seismic image to obtain a more geologically reasonable surface. However, we need not manually interpret the entire horizon. Using a small number of control points as constraints, we solve a constrained least-squares problem to efficiently and accurately extract a sequence boundary or horizon from a noisy or complex seismic image.

2.3.1 Constrained optimization

As discussed above, in each iteration that updates a horiozn surface, we solve a linear system $\mathbf{Af} = \mathbf{b}$ for the vector $\mathbf{f}$ that represents the surface. Because the matrix $\mathbf{A}$ is SPD, solving this linear system is equivalent to minimizing the following quadratic function of the vector $\mathbf{f}$:

$$F(\mathbf{f}) = \frac{1}{2}\mathbf{f}^\top\mathbf{Af} - \mathbf{b}^\top\mathbf{f}. \tag{12}$$

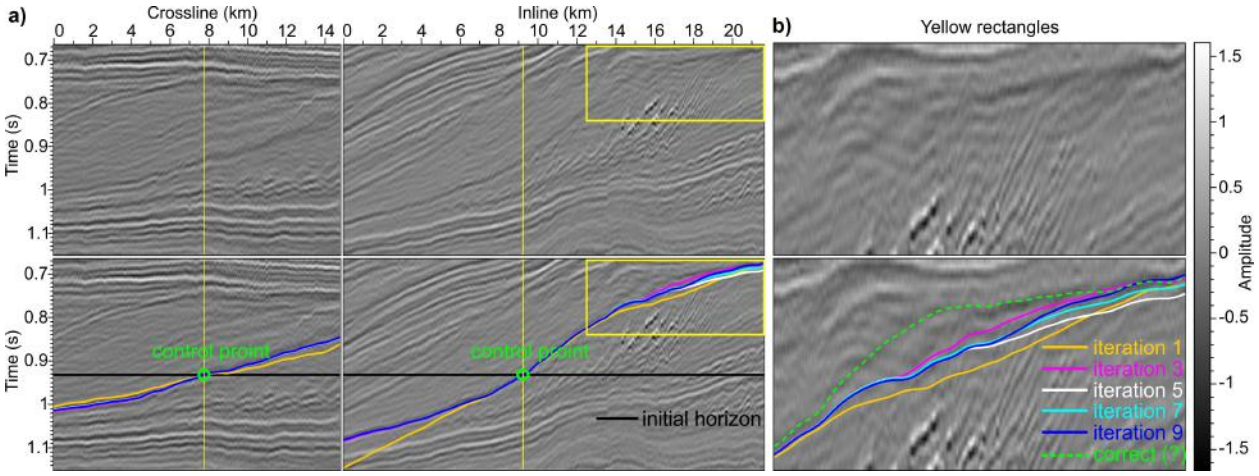

Figure 3. Seismic sections (a) and subsections (b) that intersect with a sequence boundary. The initially horizontal surface (black curve) passes through one control point and is updated iteratively using seismic normal vectors. The dashed green curve denotes the manually interpreted sequence boundary.

Suppose we have a set of n control points $(x_i, y_i, z_i), i = 1, 2, ..., n$, and we want to extract a horizon surface that exactly passes through these points. With these constraints, we obtain a constrained optimization problem:

$$\begin{aligned} &\text{minimize}_{\mathbf{f}} \quad F(\mathbf{f}) = \frac{1}{2}\mathbf{f}^\top \mathbf{A}\mathbf{f} - \mathbf{b}^\top \mathbf{f}, \\ &\text{subject to} \quad \mathbf{C}\mathbf{f} = \mathbf{z}, \end{aligned} \tag{13}$$

where $\mathbf{z} = [z_1, z_2, ..., z_n]^\top$ is an $n \times 1$ column vector, and $\mathbf{C}$ is an $n \times N$ (where, again, N is the number of depths sampled on the surface) sparse matrix with ones at the positions corresponding to control points and zeros elsewhere. Assuming we have found some solution $\mathbf{f}_0$ to the constraint equation $\mathbf{C}\mathbf{f}_0 = \mathbf{z}$, and a matrix $\mathbf{Z}$ whose columns form a basis for the null space of $\mathbf{C}$ so that $\mathbf{C}\mathbf{Z} = \mathbf{0}$, then any solution $\mathbf{f}$ of the constraint equation $\mathbf{C}\mathbf{f} = \mathbf{z}$ can be written as

$$\mathbf{f} = \mathbf{f}_0 + \mathbf{Z}\mathbf{p}, \tag{14}$$

where $\mathbf{p}$ is a reduced $(N - n) \times 1$ column vector, and again n is the number of control points. The control points must be unique to ensure that the matrix $\mathbf{C}$ has n linearly independent rows and $\mathbf{Z}$ has $N - n$ linearly independent columns.

Substituting equation 14 into equation 12, we obtain a quadratic function $F(\mathbf{p})$ with the reduced vector $\mathbf{p}$:

$$F(\mathbf{p}) = \frac{1}{2}(\mathbf{f}_0 + \mathbf{Z}\mathbf{p})^\top \mathbf{A}(\mathbf{f}_0 + \mathbf{Z}\mathbf{p}) - \mathbf{b}^\top(\mathbf{f}_0 + \mathbf{Z}\mathbf{p}). \tag{15}$$

Minimizing this quadratic function for the reduced solution $\mathbf{p}$, is equivalent to, solving the following reduced linear system

$$\mathbf{Z}^\top \mathbf{A}\mathbf{Z}\mathbf{p} = \mathbf{Z}^\top(\mathbf{b} - \mathbf{A}\mathbf{f}_0). \tag{16}$$

We can now solve this reduced system to get $\mathbf{p}$, and then recover the desired solution $\mathbf{f}$ by using equation 14.

2.3.2 Constrained preconditioner

Before we can solve equation 16, we must find matrix $\mathbf{Z}$ and vector $\mathbf{f}_0$. Fortunately, these subproblems are simple. For example, assume we have three control points: $f_0 = z_0$, $f_2 = z_2$, and $f_3 = z_3$, then $\mathbf{z} = [z_0 \ z_2 \ z_3]^\top$ and the matrix $\mathbf{C}$ is

$$\mathbf{C} = \begin{bmatrix} 1 & 0 & 0 & 0 & 0 & \cdots & 0 \\ 0 & 0 & 1 & 0 & 0 & \cdots & 0 \\ 0 & 0 & 0 & 1 & 0 & \cdots & 0 \end{bmatrix}_{3 \times N}. \tag{17}$$

We can immediately find a solution $\mathbf{f}_0 = [z_0 \ 0 \ z_2 \ z_3 \ 0 \ \cdots \ 0]^\top$ to the constraint equation $\mathbf{C}\mathbf{f}_0 = \mathbf{z}$.

The columns of matrix $\mathbf{Z}$ form a basis of the null space of matrix $\mathbf{C}$, so that $\mathbf{C}\mathbf{Z} = \mathbf{0}$. We generate such a matrix $\mathbf{Z}$ from an $N \times N$ identity matrix, by simply removing any columns that are identical to rows in the matrix $\mathbf{C}$:

$$\mathbf{Z} = \begin{bmatrix} 0 & 0 & \cdots & 0 \\ 1 & 0 & \cdots & 0 \\ 0 & 0 & \cdots & 0 \\ 0 & 0 & \cdots & 0 \\ 0 & 1 & \cdots & 0 \\ \vdots & \vdots & \ddots & \vdots \\ 0 & 0 & \cdots & 1 \end{bmatrix}_{N \times (N-3)}. \tag{18}$$

Given $\mathbf{Z}$ and the solution $\mathbf{f}_0$, we are ready to solve the reduced system shown in equation 16. Because the matrix $\mathbf{Z}^\top \mathbf{A}\mathbf{Z}$ is SPD, we can use the CG method to solve this reduced system. Many authors (e.g., Nash and Sofer, 1996; Gould et al., 2001; Dollar, 2005) have dis-

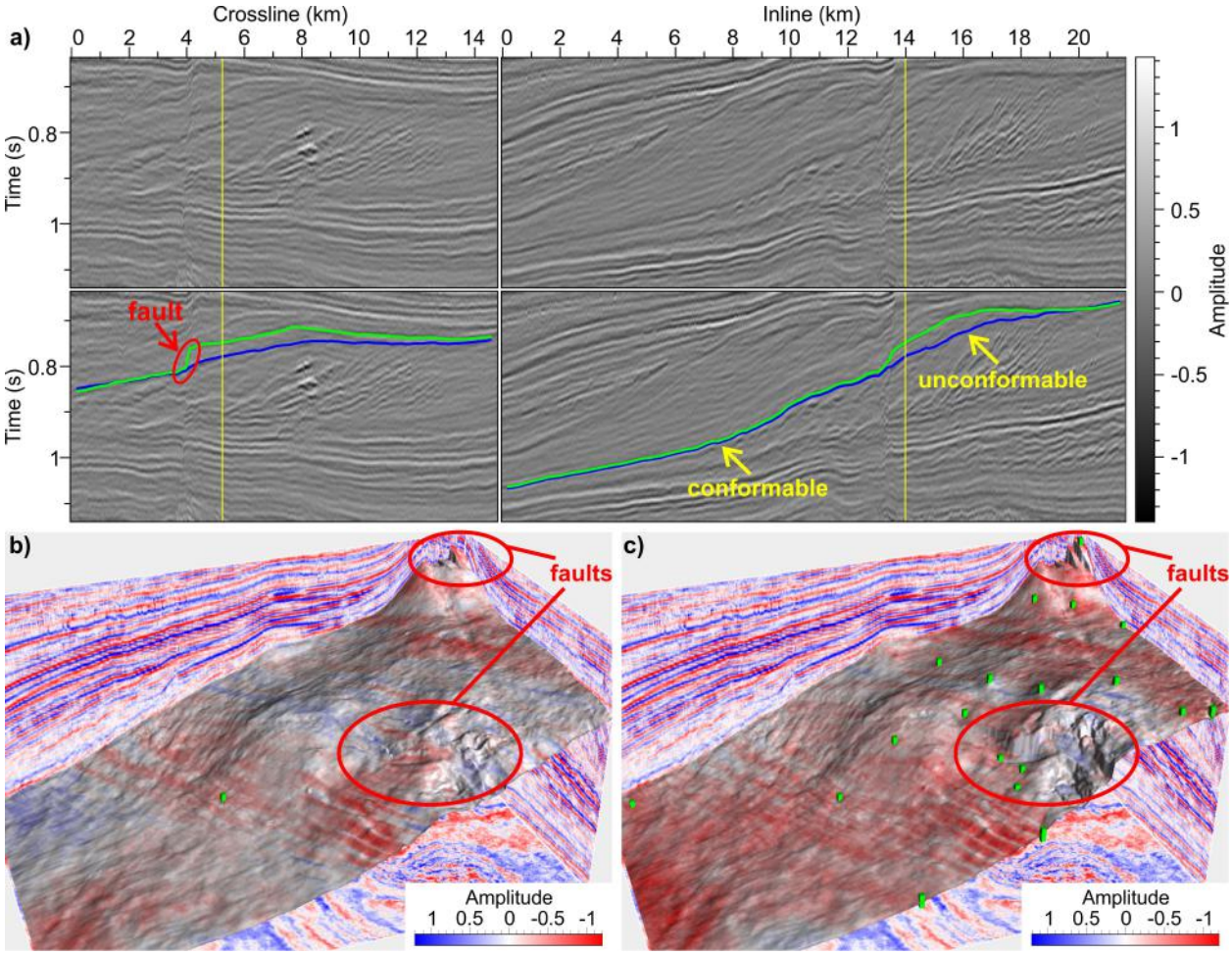

Figure 4. Seismic sections (a) intersect sequence boundaries extracted using one control point (blue curve) and 19 control points (green curve). (b) and (c) show a 3D view of the extracted surfaces using one control point and 19 control points, respectively.

cussed the solution of this system using the preconditioned CG method. In this paper, we use a simple preconditioner $\mathbf{P}_z$ described in Nash and Sofer (1996):

$$\mathbf{P}_z = \mathbf{Z}^\top \mathbf{M}^{-1}\mathbf{Z} \approx (\mathbf{Z}^\top \mathbf{A}\mathbf{Z})^{-1}, \tag{19}$$

where $\mathbf{M}^{-1} = \mathbf{S}_x\mathbf{S}_y\mathbf{S}_y^\top\mathbf{S}_x^\top$ as in equation 11, and $\mathbf{Z}^\top\mathbf{Z} = \mathbf{I}$ since the columns of $\mathbf{Z}$ form a basis. Therefore, our preconditioner for the reduced system is

$$\mathbf{P}_z = \mathbf{Z}^\top\mathbf{S}_x\mathbf{S}_y\mathbf{S}_y^\top\mathbf{S}_x^\top\mathbf{Z}. \tag{20}$$

In the preconditioned CG method for the reduced system, one would compute the initial residual $\mathbf{r}_z = \mathbf{Z}^\top(\mathbf{b}-\mathbf{A}\mathbf{f}_0) - \mathbf{Z}^\top\mathbf{A}\mathbf{Z}\mathbf{p}$ and the preconditioned residual $\mathbf{g}_z = \mathbf{P}_z\mathbf{r}_z$.

Instead of solving the reduced system to obtain $\mathbf{p}$ and then recovering the desired solution $\mathbf{f}$, we can instead directly solve for $\mathbf{f}$ because we have a relationship between the reduced and full solutions $\mathbf{f} = \mathbf{f}_0 + \mathbf{Z}\mathbf{p}$. As discussed by Gould et al. (2001), to explicitly perform the multiplication by $\mathbf{Z}$ and the addition of the term $\mathbf{f}_0$ in the CG method, we may choose $\mathbf{f} = \mathbf{f}_0 + \mathbf{Z}\mathbf{p}$, $\mathbf{Z}^\top\mathbf{r} = \mathbf{r}_z$ and $\mathbf{g} = \mathbf{Z}\mathbf{g}_z$, so that $\mathbf{g} = \mathbf{Z}\mathbf{P}_z\mathbf{Z}^\top\mathbf{r}$. This process is equivalent to applying the preconditioned CG method to the unconstrained linear system $\mathbf{A}\mathbf{f} = \mathbf{b}$, with a preconditioner

$$\mathbf{P} = \mathbf{Z}\mathbf{P}_z\mathbf{Z}^\top = \mathbf{Z}\mathbf{Z}^\top\mathbf{M}^{-1}\mathbf{Z}\mathbf{Z}^\top = \mathbf{Z}\mathbf{Z}^\top\mathbf{S}_x\mathbf{S}_y\mathbf{S}_y^\top\mathbf{S}_x^\top\mathbf{Z}\mathbf{Z}^\top. \tag{21}$$

In practice, we do not explicitly form the matrices $\mathbf{A}$ and $\mathbf{Z}\mathbf{Z}^\top$ because the preconditioned CG method requires only the computation of the residual vector $\mathbf{r} = \mathbf{b} - \mathbf{A}\mathbf{f}$ and gradient vector $\mathbf{g} = \mathbf{P}\mathbf{r}$.

It is trivial to compute vector $\mathbf{Z}\mathbf{Z}^\top\mathbf{x}$ for any $N \times 1$

vector $\mathbf{x}$ because $\mathbf{Z}\mathbf{Z}^\top$ has the form

$$\mathbf{Z}\mathbf{Z}^\top = \begin{bmatrix} 0 & 0 & 0 & 0 & 0 & \cdots & 0 \\ 0 & 1 & 0 & 0 & 0 & \cdots & 0 \\ 0 & 0 & 0 & 0 & 0 & \cdots & 0 \\ 0 & 0 & 0 & 0 & 0 & \cdots & 0 \\ 0 & 0 & 0 & 0 & 1 & \cdots & 0 \\ \vdots & \vdots & \vdots & \vdots & \vdots & \ddots & \vdots \\ 0 & 0 & 0 & 0 & 0 & \cdots & 1 \end{bmatrix}_{N \times N}. \quad (22)$$

Computation of $\mathbf{Z}\mathbf{Z}^\top\mathbf{x}$ simply zeros all the elements of $\mathbf{x}$ with indices corresponding to the locations of control points.

With the preconditioner $\mathbf{P}$ denoted by equation 21, the preconditioned gradient $\mathbf{g} = \mathbf{Z}\mathbf{g}_z = \mathbf{Z}\mathbf{P}_z\mathbf{Z}^\top\mathbf{r}$ is projected to be in the null space of $\mathbf{C}$. As a result, all updates to the solution $\mathbf{f}$ in this preconditioned CG method will also lie in the null space of $\mathbf{C}$. Therefore, because the initial solution $\mathbf{f}_0$ satisfies the constraints $\mathbf{C}\mathbf{f}_0 = \mathbf{z}$, the solution $\mathbf{f}$ after each CG iteration also satisfies $\mathbf{C}\mathbf{f} = \mathbf{z}$.

2.4 Results with constraints

Where seismic normal vectors estimated from structure tensors are inaccurate (e.g., near unconformities, faults and noisy data), the use of control points helps to extract a more reliable horizon or sequence boundary. As shown in Figure 3, when we extract a sequence boundary constrained by only one control point (green circle in Figure 3a), the surface we extract (blue curves in Figure 3) is well aligned with a seismic reflector in the conformable areas (the left-side section and the left part of the right-side section in Figure 3a), where seismic normal vectors can be estimated accurately. However, the surface (blue curves) extracted at the unconformity (Figure 3b) deviates from the correct surface (dashed green curve in Figure 3b) because the normal vectors estimated there are inaccurate.

Using 19 control points (green points in Figure 4c), we obtain a more accurate sequence boundary. Figure 4a shows crossline and inline seismic sections that intersect the sequence boundaries extracted using (1) only one control point (blue curves), and (2) 19 control points (green curves). We observe that the sequence boundary extracted using 19 control points correctly represents the unconformity, while the one extracted using only one control point does not. Figures 4b and 4c show the same extracted sequence-boundary surfaces colored with seismic amplitudes. Amplitude values for 19 control points (Figure 4c) are more uniform than those for one control point (Figure 4b).

Note that this sequence boundary is also complicated by faults, highlighted by red ellipses in Figure 4. The surface extracted using only 1 control point (blue curves in Figure 4a and the surface in Figure 4b) is inaccurate near faults. However, the surface with 19 control points (green curves in Figure 4a and the surface in Figure 4c) correctly follows the faults. This example demonstrates that constraints facilitate extraction of a horizon surface complicated by faults.

Moreover, with more control points, an initially horizontal surface converges more quickly to the final extracted horizon. We can use more control points to interpolate a better initial surface $f^0(x, y)$ that is closer to the seismic horizon $f(x, y)$ we want to extract, which therefore enables the CG method to more quickly converge to that horizon. For example, it takes nine iterations to converge using one control point (blue curves in Figure 4)a, but only five iterations to converge using 19 control points (green curves in Figure 4)a.

3 GENERATING A HORIZON VOLUME

Using the method discussed above, we can extract a single seismic horizon or sequence boundary with one or more control points that represent interpreted constraints. With similar constraints, we can also extract all seismic horizons from a seismic image at once, and thereby generate a complete horizon volume. In a horizon volume $z(x, y, \tau)$, as shown in Figure 2c, the vertical axis is RGT τ and color denotes depth z. Horizontally slicing a horizon volume at any single RGT value τ yields a seismic horizon.

Here, we first describe a method for using seismic normal vectors to automatically generate a horizon volume without constraints, which is usually accurate for seismic images with simple structures. To better handle images complicated by faults or noise, we then extend this method, by incorporating scattered sets of points that correspond to multiple seismic horizons, to generate a more reliable horizon volume that honors those interpreted constraints.

3.1 Horizon volume without constraints

As discussed by Parks (2010), a horizon volume $z(x, y, \tau)$ can be generated from an RGT volume $\tau(x, y, z)$ by inverse linear interpolation if we assume that τ in the RGT volume increases monotonically with depth z. Some authors have described methods to generate such an RGT volume using phase unwrapping (e.g., Stark, 2005; Wu and Zhong, 2012b) or reflector dips (Parks, 2010). Here we rederive the latter method in a simpler way to compute an RGT volume.

In an RGT volume $\tau(x, y, z)$ like that shown in Figure 5a or 2b, contours (Figure 5b) of constant τ represent seismic horizons, which means these contours should have the same structures as seismic reflectors in the seismic image (Figure 5b). Therefore, gradient vectors for an RGT volume $\tau(x, y, z)$, that are perpendicular to RGT contours, should be parallel to seismic normal vectors $\mathbf{n} = [n_x, n_y, n_z]^\top$, that are perpendicular to seismic reflectors. If we assume that these vectors

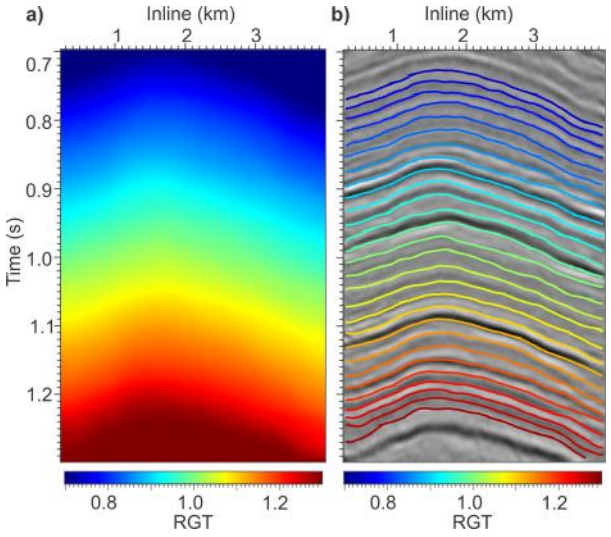

Figure 5. The same RGT volume (a) as shown in Figure 2b, contours (b) of the RGT volume are horizons in the corresponding seismic image.

always point downward, we have

$$\begin{bmatrix} \frac{\partial \tau}{\partial x} \\ \\ \frac{\partial \tau}{\partial y} \\ \\ \frac{\partial \tau}{\partial z} \end{bmatrix} \approx \alpha \begin{bmatrix} n_x \\ \\ n_y \\ \\ n_z \end{bmatrix}, \tag{23}$$

where α is a positive scalar constant. Because we again have more equations than unknowns, in general we can only approximately solve these coupled partial differential equations.

To eliminate α, we let $\partial\tau/\partial z = \alpha n_z$ to obtain

$$\begin{bmatrix} n_z \frac{\partial \tau}{\partial x} - n_x \frac{\partial \tau}{\partial z} \\ \\ n_z \frac{\partial \tau}{\partial y} - n_y \frac{\partial \tau}{\partial z} \end{bmatrix} \approx \begin{bmatrix} 0 \\ \\ 0 \end{bmatrix}. \tag{24}$$

In attempting to solve these equations, we would need to carefully choose boundary conditions to avoid obtaining the trivial solution $\tau = constant$.

To avoid this problem, as discussed by Parks (2010), we rewrite $\tau(x,y,z)$ as

$$\tau(x,y,z) = z + s(x,y,z), \tag{25}$$

where the function $s(x,y,z)$ represents vertical shifts. Substituting equation 25 into equation 24, we obtain

$$\begin{bmatrix} n_z \frac{\partial s}{\partial x} - n_x \frac{\partial s}{\partial z} \\ \\ n_z \frac{\partial s}{\partial y} - n_y \frac{\partial s}{\partial z} \end{bmatrix} \approx \begin{bmatrix} n_x \\ \\ n_y \end{bmatrix}, \tag{26}$$

or

$$\begin{bmatrix} -\frac{\partial s}{\partial x} - p \frac{\partial s}{\partial z} \\ \\ -\frac{\partial s}{\partial y} - q \frac{\partial s}{\partial z} \end{bmatrix} \approx \begin{bmatrix} p \\ \\ q \end{bmatrix}, \tag{27}$$

where again $p = -n_x/n_z$ and $q = -n_y/n_z$ are estimated inline and crossline slopes of seismic reflectors. Equation 27 is what Parks (2010) solved to obtain shifts that flatten a seismic image.

As suggested by Lomask et al. (2006), we add a third equation $\epsilon s_z \approx 0$ to reduce vertical variations in the shifts. We also weight the equations above by a measure $w(x,y,z)$ of the quality of the estimated reflector slopes $p(x,y,z)$ and $q(x,y,z)$. We then compute the shifts by solving the following equations:

$$\begin{bmatrix} w(-\frac{\partial s}{\partial x} - p\frac{\partial s}{\partial z}) \\ \\ w(-\frac{\partial s}{\partial y} - p\frac{\partial s}{\partial z}) \\ \\ \epsilon \frac{\partial s}{\partial z} \end{bmatrix} \approx \begin{bmatrix} wp \\ \\ wq \\ \\ 0 \end{bmatrix}. \tag{28}$$

If we have N image samples, then equation 28 represents $3N$ equations for N unknown shifts, and these equations can be expressed in matrix form as

$$\mathbf{WGs} = \mathbf{Wv}, \tag{29}$$

where $\mathbf{s}$ is an $N \times 1$ vector containing the unknown shifts $s(x,y,z)$, $\mathbf{G}$ is a $3N \times N$ sparse matrix representing finite-difference approximations of partial derivatives, $\mathbf{W}$ is a $3N \times 3N$ diagonal matrix containing weights $w(x,y,z)$ and the constant ϵ, and $\mathbf{v}$ is a $3N \times 1$ vector with $2N$ slopes p and q, and N zeros.

We compute the least-squares solution to equation 29 by solving the normal equations

$$(\mathbf{WG})^\top \mathbf{WGs} = (\mathbf{WG})^\top \mathbf{Wv}. \tag{30}$$

Let $\mathbf{A} = (\mathbf{WG})^\top \mathbf{WG}$ and $\mathbf{b} = (\mathbf{WG})^\top \mathbf{Wv}$ so that this linear system becomes

$$\mathbf{As} = \mathbf{b}. \tag{31}$$

The matrix $\mathbf{A}$ is both SPD and sparse. In practice, we do not explicitly form the matrices $\mathbf{A}$, $\mathbf{W}$, and $\mathbf{G}$. Instead, we solve this linear system using the CG method, which requires only the computation of matrix-vector products like $\mathbf{As} = (\mathbf{WG})^\top \mathbf{WGs}$ and $\mathbf{b} = (\mathbf{WG})^\top \mathbf{Wv}$.

As when extracting a single seismic horizon, we solve equation 31 using the preconditioned CG method with a preconditioner defined by

$$\mathbf{M^{-1}} = \mathbf{S}_x\mathbf{S}_y\mathbf{S}_z\mathbf{S}_z^\top\mathbf{S}_y^\top\mathbf{S}_x^\top, \tag{32}$$

where, again, $\mathbf{S}_x$, $\mathbf{S}_y$ and $\mathbf{S}_z$ are filters that smooth in the x, y and z directions, respectively. We again expect the solution to be laterally smooth except at faults, as shown in Figure 7b. Therefore, the lateral smoothing filters $\mathbf{S}_x$ and $\mathbf{S}_y$ are spatially variant filters (Hale, 2009), and the extent of smoothing is proportional to a measure of reflector continuity, so that these filters smooth less at faults. In this example, we expect the shifts to be smooth vertically because we do not have unconformities. Therefore, our vertical smoothing filter $\mathbf{S}_z$ in this example is spatially invariant.

Note that we derive all of the equations above for

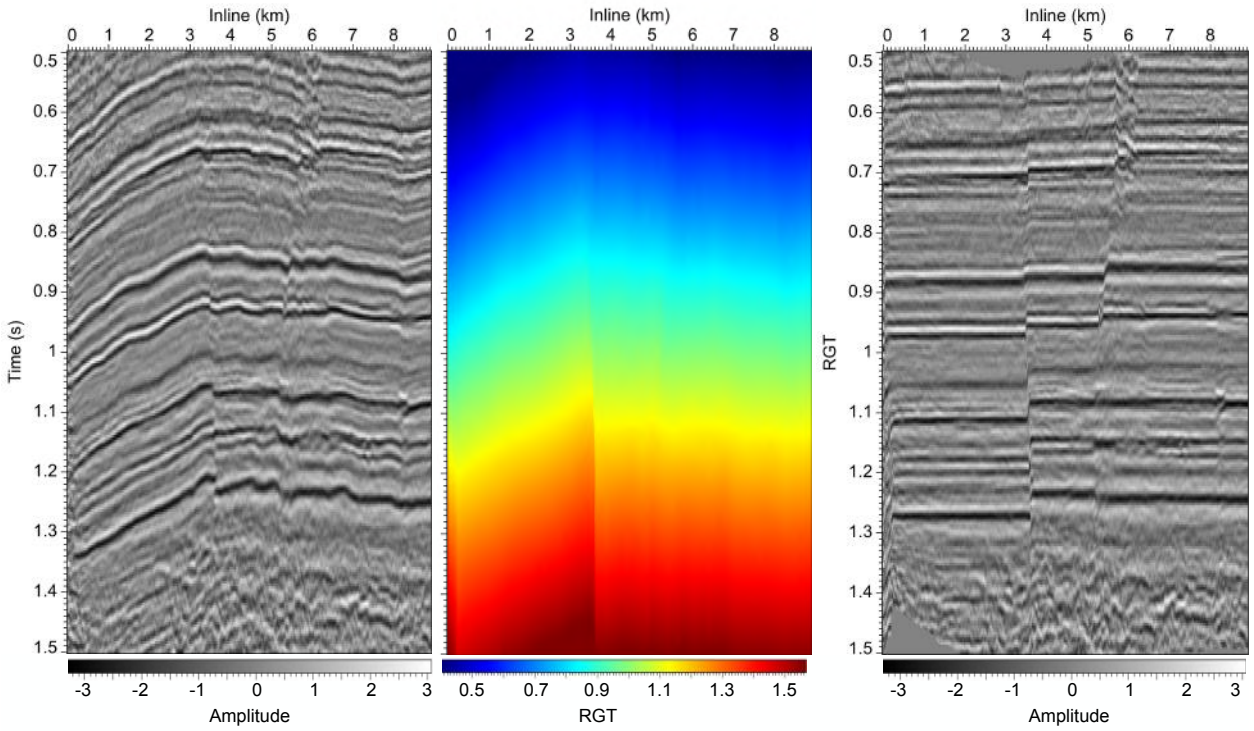

Figure 6. A seismic image (a), generated RGT volume (b), and flattened image (c) without control points.

3D images, but they can be easily modified to work for 2D images, by simply omitting the second equation for the y direction from equation 28. For the 2D example shown in Figure 2, we first solved equation 31 to get shifts $s(x, z)$. We then computed an RGT volume $\tau(x, z) = z + s(x, z)$ (Figure 2b), where τ increases monotonically with depth z. Finally we computed a horizon volume $z(x, \tau)$ (Figure 2c) from the RGT volume $\tau(x, z)$ by inverse linear interpolation (Parks, 2010). This horizon volume $z(x, \tau)$ maps the seismic image (Figure 2a) to a flattened image (Figure 2d).

For seismic images with simple geologic structures and little noise, as in Figure 2a, we can use the method discussed above to compute an accurate RGT volume (Figure 2b) and then interpolate a horizon volume (Figure 2c) that well flattens (Figure 2d) a seismic image. However, for seismic images complicated by faults, as in Figure 6a, the generated RGT volume (Figure 6b) is inaccurate, so that seismic reflectors are not flattened correctly (Figure 6c). Therefore, we extend this method to compute more accurate RGT and horizon volumes by incorporating scattered sets of control points that may correspond to multiple horizons.

3.2 Horizon volume with constraints

For specified sets of control points, we solve a constrained optimization problem similar to that we solve when extracting a single seismic horizon:

$$\begin{aligned} &\text{minimize}_{\mathbf{s}} \quad F(\mathbf{s}) = \frac{1}{2}\mathbf{s}^\top \mathbf{A}\mathbf{s} - \mathbf{b}^\top \mathbf{s}, \\ &\text{subject to} \quad \mathbf{C}\mathbf{s} = \mathbf{d}. \end{aligned} \tag{33}$$

As when extracting a single horizon, solving the constrained problem above is equivalent to solving a corresponding unconstrained problem $\mathbf{A}\mathbf{s} = \mathbf{b}$ using a preconditioned CG method with an initial solution $\mathbf{s}_0$ to the constraint equation $\mathbf{C}\mathbf{s}_0 = \mathbf{d}$ and a constrained preconditioner $\mathbf{P} = \mathbf{Z}\mathbf{Z}^\top \mathbf{M}^{-1} \mathbf{Z}\mathbf{Z}^\top$, where $\mathbf{M}^{-1} = \mathbf{S}_x \mathbf{S}_y \mathbf{S}_z \mathbf{S}_z^\top \mathbf{S}_y^\top \mathbf{S}_x^\top$. Therefore, to solve this problem, we need only an initial solution $\mathbf{s}_0$ and the matrix $\mathbf{Z}\mathbf{Z}^\top$ for the preconditioner $\mathbf{P}$.

Let us use a tiny 3D seismic image with only $N = 2 \times 2 \times 2$ samples to explain how to implement multiplication by the matrix $\mathbf{Z}\mathbf{Z}^\top$ and to find an initial solution $\mathbf{s}_0$. As in equation 25, we want to compute a 3D RGT volume $\tau(x, y, z)$ with shifts $s(x, y, z)$. In this simple example, both τ and s have only $N = 2 \times 2 \times 2$ samples, and we can express equation 25 in vector form as

$$\boldsymbol{\tau} = \mathbf{z} + \mathbf{s}, \tag{34}$$

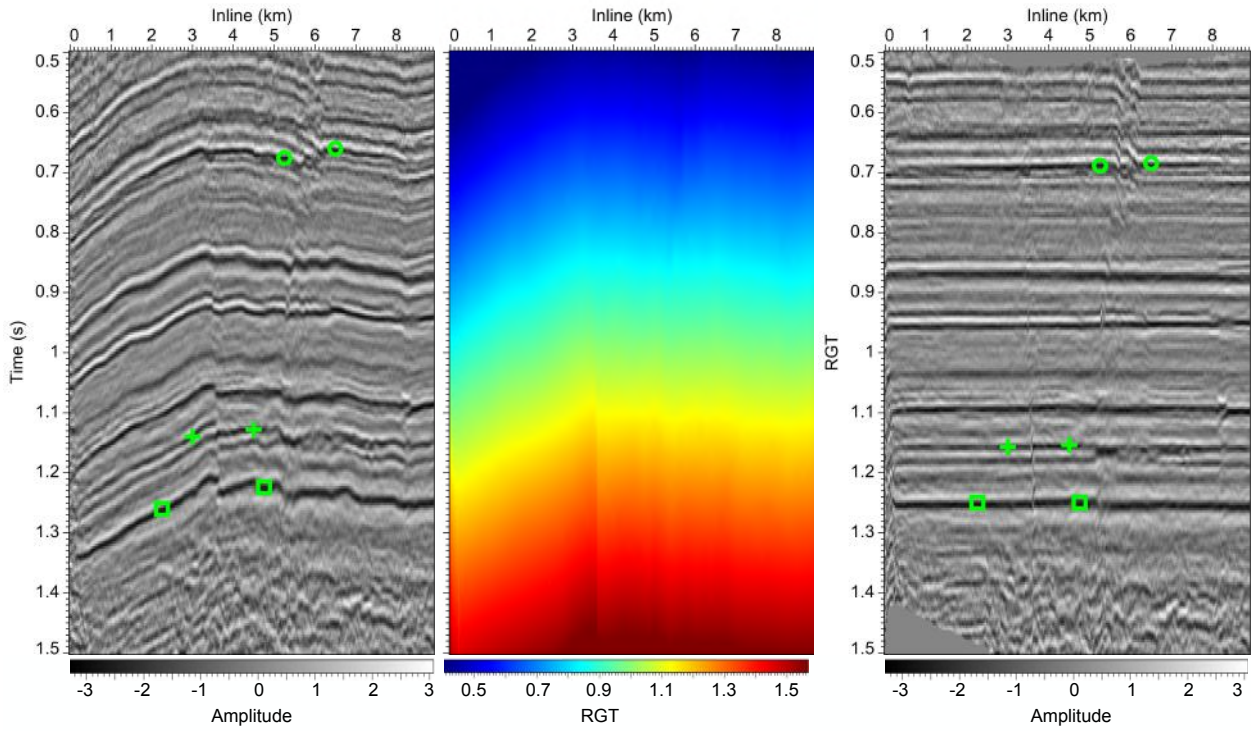

Figure 7. A seismic image (a) with 3 pairs of interactively interpreted control points (green circles, pluses and squares), generated RGT volume (b) and flattened image (c).

where

$$\begin{aligned}\boldsymbol{\tau} &= [\tau_0\ \tau_1\ \tau_2\ \tau_3\ \tau_4\ \tau_5\ \tau_6\ \tau_7]^\top,\\ \mathbf{z} &= [z_0\ z_1\ z_2\ z_3\ z_4\ z_5\ z_6\ z_7]^\top,\\ \mathbf{s} &= [s_0\ s_1\ s_2\ s_3\ s_4\ s_5\ s_6\ s_7]^\top.\end{aligned} \tag{35}$$

Assume that we have 2 sets of constraints: the first set has 3 control points with sample indices $\{3,5,7\}$, and the second set has 2 control points with sample indices $\{1,6\}$. Within each set of constraints, all control points are interpreted to be on a single seismic horizon. Therefore, we have $\tau_3=\tau_5=\tau_7$ and $\tau_1=\tau_6$. According to equation 34, this means that $s_5-s_3=z_3-z_5$ and $s_7-s_3=z_3-z_7$, and $s_6-s_1=z_1-z_6$. We can therefore write the constraint equation $\mathbf{Cs}=\mathbf{d}$ as follows:

$$\begin{bmatrix}0&0&0&-1&0&1&0&0\\0&0&0&-1&0&0&0&1\\0&-1&0&0&0&0&1&0\end{bmatrix}\mathbf{s}=\begin{bmatrix}z_3-z_5\\z_3-z_7\\z_1-z_6\end{bmatrix}, \tag{36}$$

where, again, $\mathbf{s}=[s_0\ s_1\ s_2\ s_3\ s_4\ s_5\ s_6\ s_7]^\top$.

In this example, matrix $\mathbf{C}$ has 3 linearly independent rows so that matrix $\mathbf{Z}$ must have $N-3$ linearly independent columns, such that $\mathbf{CZ}=\mathbf{0}$, because the columns of matrix $\mathbf{Z}$ form a basis for the null space of $\mathbf{C}$. Construction of matrix $\mathbf{Z}$ is only slightly more complicated than for the single-horizon case. Specifically,

$$\mathbf{Z}=\begin{bmatrix}\mathbf{e}_{c1}\mid\mathbf{e}_{c2}\mid\mathbf{e}_0\mid\mathbf{e}_2\mid\mathbf{e}_4\end{bmatrix}=\begin{bmatrix}0&0&1&0&0\\0&1&0&0&0\\0&0&0&1&0\\1&0&0&0&0\\0&0&0&0&1\\1&0&0&0&0\\0&1&0&0&0\\1&0&0&0&0\end{bmatrix}_{8\times5}, \tag{37}$$

where $\mathbf{e}_{c1}=\mathbf{e}_3+\mathbf{e}_5+\mathbf{e}_7$, $\mathbf{e}_{c2}=\mathbf{e}_1+\mathbf{e}_6$, and $\mathbf{e}_i$, for $i=0,1,\cdots,N-1$, is an $N\times1$ unit vector with 1 at the $i-th$ index. In other words, we begin with the identity matrix and simply sum the unit vectors $\mathbf{e}_i$ with indices i in $\{3,5,7\}$, corresponding to the first set of control points, to obtain the first column of $\mathbf{Z}$; similarly, we obtain the second column of $\mathbf{Z}$, corresponding to the second set of control points with indices $\{1,6\}$; and finally, we use all of the remaining unit vectors $\mathbf{e}_i$ that do not correspond to any control point for remaining columns of $\mathbf{Z}$. In the same way, we can easily construct matrix $\mathbf{Z}$ for any number of sets of control points.

We can normalize the columns of matrix $\mathbf{Z}$ to ob-

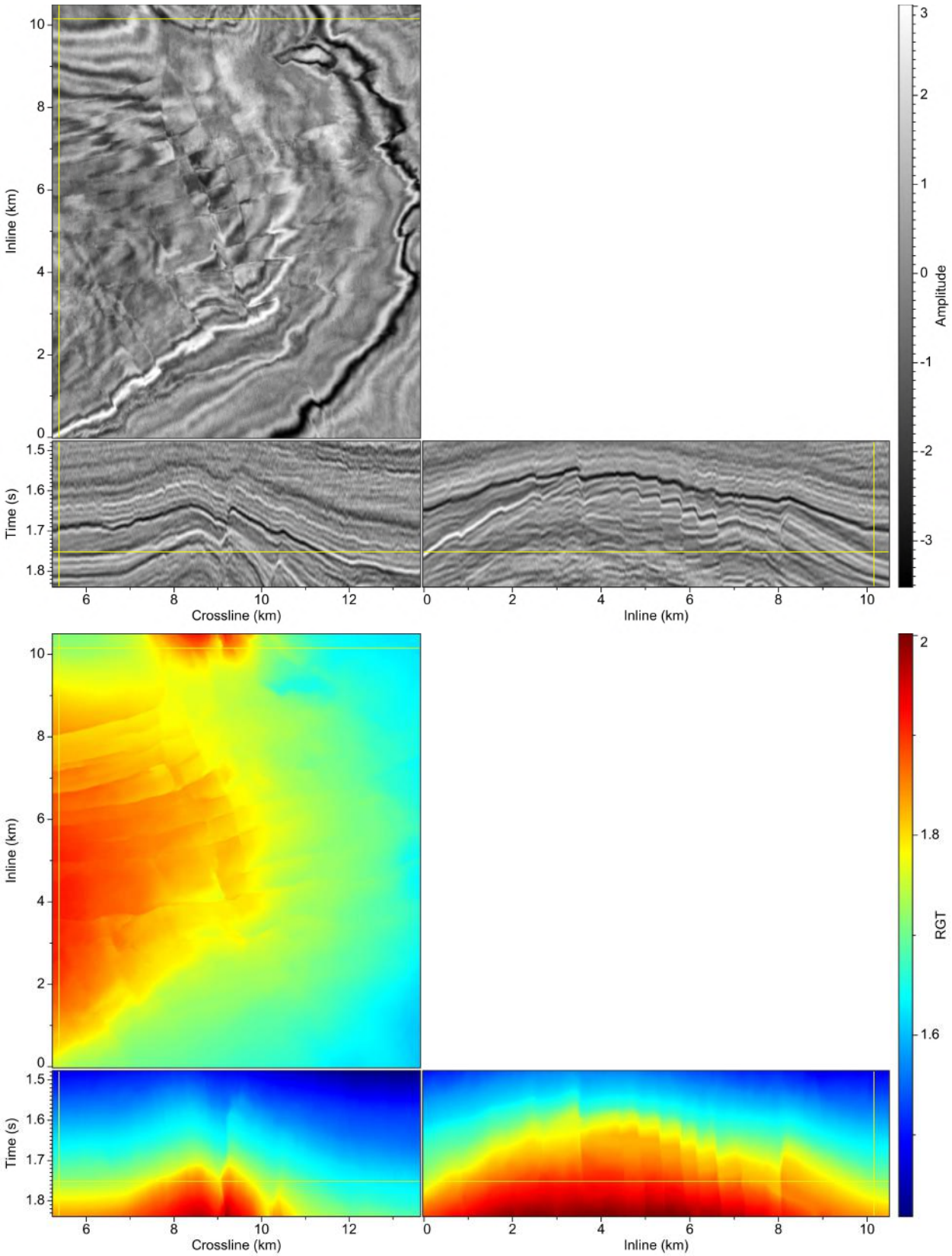

Figure 8. Input seismic image (a) and a corresponding RGT volume (b) computed with three sets of control points.

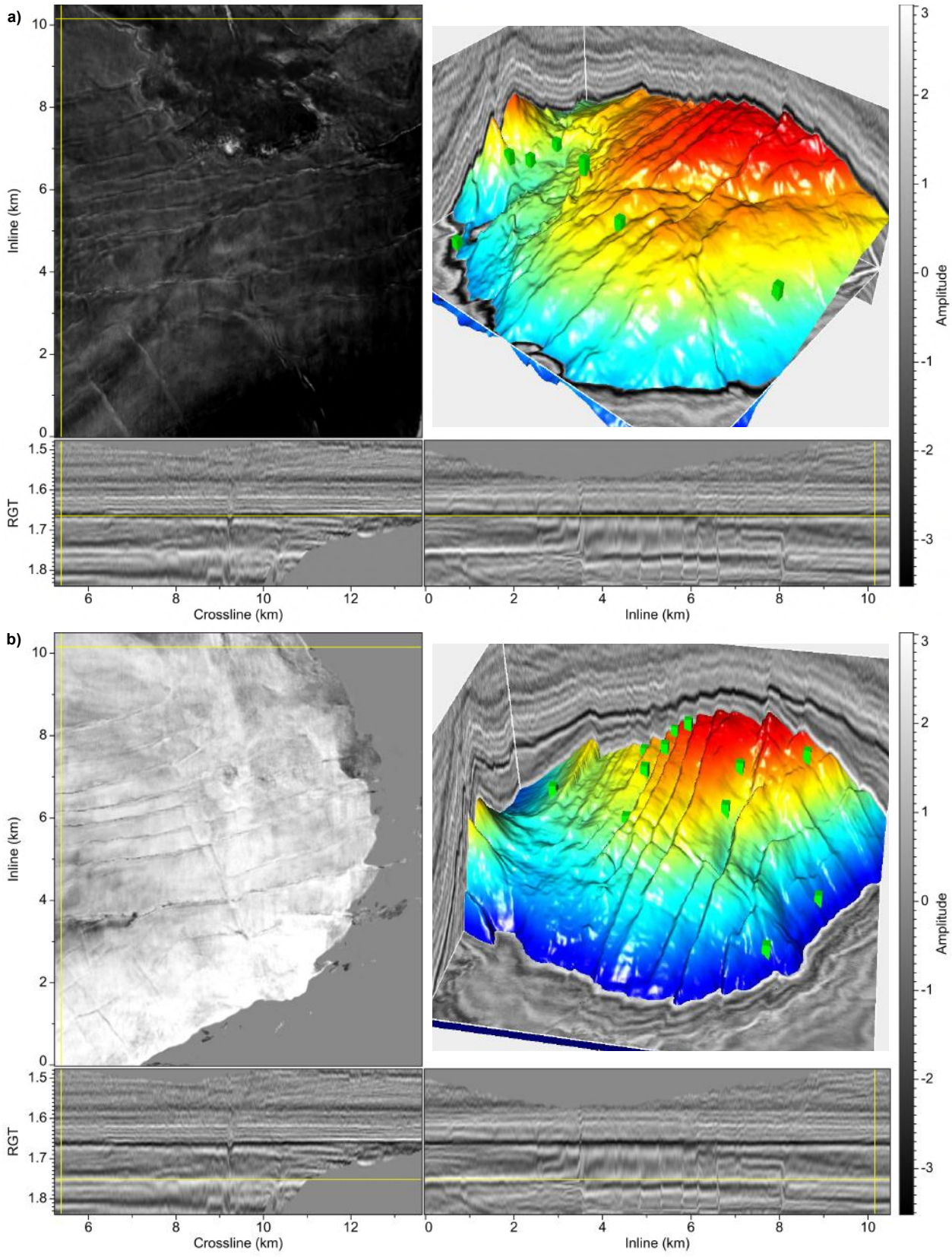

Figure 9. The flattened seismic image is sliced at $\tau = 1.664$ (a) and $\tau = 1.751$ (b). Horizontal slices in a flattened image correspond to seismic horizon surfaces (upper-right panels in (a) and (b), for which color denotes depth) in an unflattened image.

tain

$$\mathbf{Z} = \begin{bmatrix} 0 & 0 & 1 & 0 & 0 \\ 0 & \frac{1}{\sqrt{2}} & 0 & 0 & 0 \\ 0 & 0 & 0 & 1 & 0 \\ \frac{1}{\sqrt{3}} & 0 & 0 & 0 & 0 \\ 0 & 0 & 0 & 0 & 1 \\ \frac{1}{\sqrt{3}} & 0 & 0 & 0 & 0 \\ 0 & \frac{1}{\sqrt{2}} & 0 & 0 & 0 \\ \frac{1}{\sqrt{3}} & 0 & 0 & 0 & 0 \end{bmatrix}_{8\times 5} \tag{38}$$

with columns that form an orthonormal basis for the null space of matrix $\mathbf{C}$.

We then find that

$$\mathbf{Z}\mathbf{Z}^\top = \begin{bmatrix} 1 & 0 & 0 & 0 & 0 & 0 & 0 & 0 \\ 0 & \frac{1}{2} & 0 & 0 & 0 & 0 & \frac{1}{2} & 0 \\ 0 & 0 & 1 & 0 & 0 & 0 & 0 & 0 \\ 0 & 0 & 0 & \frac{1}{3} & 0 & \frac{1}{3} & 0 & \frac{1}{3} \\ 0 & 0 & 0 & 0 & 1 & 0 & 0 & 0 \\ 0 & 0 & 0 & \frac{1}{3} & 0 & \frac{1}{3} & 0 & \frac{1}{3} \\ 0 & \frac{1}{2} & 0 & 0 & 0 & 0 & \frac{1}{2} & 0 \\ 0 & 0 & 0 & \frac{1}{3} & 0 & \frac{1}{3} & 0 & \frac{1}{3} \end{bmatrix}_{8\times 8}. \tag{39}$$

For any vector $\mathbf{x} = [x_0\ x_1\ x_2\ x_3\ x_4\ x_5\ x_6\ x_7]^\top$, it is easy to compute the product

$$\mathbf{Z}\mathbf{Z}^\top\mathbf{x} = [x_0\ x_{c2}\ x_2\ x_{c1}\ x_4\ x_{c1}\ x_{c2}\ x_{c1}]^\top, \tag{40}$$

where $x_{c1} = (x_3 + x_5 + x_7)/3$ and $x_{c2} = (x_1 + x_6)/2$. In other words, we compute $\mathbf{Z}\mathbf{Z}^\top\mathbf{x}$ by simply gathering and averaging all elements of $\mathbf{x}$ with indices corresponding to each set of control points, and then scattering the averages back into those same elements. In each CG iteration, when we apply the constrained preconditioner $\mathbf{P} = \mathbf{Z}\mathbf{Z}^\top\mathbf{S}_x\mathbf{S}_y\mathbf{S}_z\mathbf{S}_z^\top\mathbf{S}_y^\top\mathbf{S}_x^\top\mathbf{Z}\mathbf{Z}^\top$ to a vector, we need only compute averages and apply smoothing filters.

We can also easily find an initial solution $\mathbf{s_0}$ to the constraint equation $\mathbf{C}\mathbf{s_0} = \mathbf{d}$:

$$\mathbf{s_0} = [0\ s_1\ 0\ s_3\ 0\ s_5\ s_6\ s_7]^\top, \tag{41}$$

in which elements with indices corresponding to the first set of control points are $s_3 = 0$, $s_5 = z_3 - z_5$ and $s_7 = z_3 - z_7$; elements corresponding to the second set of control points are $s_1 = 0$ and $s_6 = z_1 - z_6$. Therefore, to construct an initial set of shifts $\mathbf{s}_0$, we use zeros for elements that do not correspond to any control points; for each set of control points, we choose any point among them as a reference point with zero shift (e.g., $s_3 = 0$ for the first set of control points, and $s_1 = 0$ for the second set of control points), and use the depth differences between the reference point and other control points for the remaining initial shifts in $\mathbf{s}_0$.

We instead construct the initial shifts $\mathbf{s}_0$ in a slightly different way. We first compute the average depth for each set of control points, and then choose the point with depth nearest to that average as the reference point. In practice, we find that this alternative $\mathbf{s}_0$ reduces the number of iterations required by the preconditioned CG method.

With an initial solution $\mathbf{s}_0$ and the constrained preconditioner $\mathbf{P} = \mathbf{Z}\mathbf{Z}^\top\mathbf{M}^{-1}\mathbf{Z}\mathbf{Z}^\top$, we can apply the preconditioned CG method to the unconstrained system $\mathbf{A}\mathbf{s} = \mathbf{b}$ to obtain a solution $\mathbf{s}$ that satisfies the constrained problem of equation 33. In each CG iteration, we compute a residual as $\mathbf{r} = \mathbf{b} - \mathbf{A}\mathbf{s}$. Using the constrained preconditioner $\mathbf{P}$, we compute a constrained residual $\mathbf{r}_P = \mathbf{Z}\mathbf{Z}^\top\mathbf{M}^{-1}\mathbf{Z}\mathbf{Z}^\top\mathbf{r}$ that is in the null space of the constraint matrix $\mathbf{C}$. This means that all of the updates to the initial solution $\mathbf{s}_0$ in this preconditioned CG method will also be in the null space of $\mathbf{C}$. Therefore, because the initial solution $\mathbf{s}_0$ satisfies the constraint equation $\mathbf{C}\mathbf{s}_0 = \mathbf{d}$, the final solution $\mathbf{s}$ obtained after any number of CG iterations will also satisfy the constraints.

Figure 7 is a 2D example that shows how constraints help to generate a more accurate horizon volume and better flatten a seismic image. In this example, we use the same input seismic image (Figure 7a) complicated by faults that is displayed in Figure 6a, but now we have 3 sets of constraints. For each set of constraints, we interpret 2 control points (green circles, pluses, and squares in Figure 7a) to lie on a seismic horizon. Figure 7b is the computed RGT volume, with which we interpolate a horizon volume that correctly flattens (Figure 7c) seismic reflectors across faults.

3.3 3D results with constraints

Figure 8a shows a 3D seismic image that is also complicated by faults. To flatten this 3D image or generate a horizon volume, we choose weights $w(x, y, z)$ corresponding to faults in equation 28. Specifically, we use the method developed by Hale (2013) to first compute an image of fault likelihoods $f(x, y, z) \in [0, 1]$ in which values near 1 indicate fault locations. We then use $w = (1 - f)^8$ as weights in equation 28.

For this example, we use three sets of constraints, corresponding to three horizons in the 3D seismic image, to compute an accurate horizon volume and correctly flatten the seismic image. The first set contains 5 control points, the second one contains 7 control points (green points in Figure 9a), and the third one contains 11 control points (green points in Figure 9b). Using these three sets of constraints, we first compute an RGT volume as shown in Figure 8b, from which we then interpolate a horizon volume that correctly flattens (Figure 9a or 9b) seismic reflectors across faults. Note that the constraints help to flatten not only reflectors passing through the control points, but also other reflectors in the 3D seismic image as well.

Figure 1 displays a 3D view of 6 seismic horizons extracted from the horizon volume computed with constraints. In Figure 1a, different colors denote different seismic horizons, but deeper horizons are obscured by the top one. We therefore, in Figure 1b, display cutaway views of each of the horizons. We observe that the

horizons with control points (the cyan and yellow surfaces) and others without control points coincide well with seismic reflectors.

4 CONCLUSION

We propose methods to (1) extract one seismic horizon at a time and (2) to compute at once a complete horizon volume. We designed these two methods to compute horizons that honor interpreted constraints, specified as sets of control points. We incorporate the control points with simple constraint preconditioners in the CG method used to compute horizons.

The first method is useful, even though we can extract all horizons at once using the second method, because it can more quickly extract a single horizon. Using multiple control points, this method can reliably extract complicated geologic surfaces such as sequence boundaries and horizons with faults. Furthermore, this first method might be used to efficiently extract horizons that might serve as control surfaces (large sets of control points) for the second method.

The second method generates a complete horizon volume at once. With a small number of interpreted constraints, this method works well for seismic images complicated by faults.

Interpreted constraints are necessary, because completely automatic interpretation cannot yet handle complicated seismic horizons. The proposed methods provide an especially simple way to specify such constraints by simply interactively picking points in a 3D seismic image that belong to the same seismic horizon. These methods can be implemented to interactively add or move control points, while quickly updating a single seismic horizon or complete horizon volume.

These methods might be further improved if we could predict areas where control points are required to generate more reliable results so that the interpretation of constraints could be more straightforward and efficient.

ACKNOWLEDGMENTS

This research is supported by the sponsor companies of the Consortium Project on Seismic Inverse Methods for Complex Structures. Seismic images shown in this paper were provided by the US Department of Energy and by dGB Earth Sciences.

REFERENCES

Dollar, H., 2005, Iterative linear algebra for constrained optimization: Ph.D. Thesis, University of Oxford.

Farnebäck, G., J. Rydell, T. Ebbers, M. Andersson, and H. Knutsson, 2007, Efficient computation of the inverse gradient on irregular domains: 2007 IEEE 11th International Conference on Computuer Vision, Vols 1-6, IEEE, 2710–2717.

Gould, N. I. M., M. E. Hribar, and J. Nocedal, 2001, On the solution of equality constrained quadratic programming problems arising in optimization: SIAM J. Sci. Comput., **23**, 1376–1395.

Hale, D., 2009, Structure-oriented smoothing and semblance: CWP Report 635.

———, 2013, Methods to compute fault images, extract fault surfaces, and estimate fault throws from 3d seismic images: Geophysics, **78**, O33–O43.

Harlan, W. S., 1995, Regularization by model reparameterization: http://www.billharlan.com/papers/regularization.pdf.

Lomask, J., 2010a, Method for determinint geological information related to a subsurface volume of interest: U. S. Patent 7,769,545 B2.

———, 2010b, Method for indexing a subsurface for the purpose of inferring geologic information: U. S. Patent 7,769,546 B2.

———, 2013, System and method for perturbing an initial horizon-picking solution to follow local features of a volume: U. S. Patent 2013/0030710 A1.

Lomask, J., A. Guitton, S. Fomel, J. Claerbout, and A. A. Valenciano, 2006, Flattening without picking: Geophysics, **71**, 13–20.

Luo, S., and D. Hale, 2012, Unfaulting and unfolding 3D seismic images: CWP Report 722.

Fehmers, G. C., and C. Höcker, 2003, Fast structural interpretation with structure-oriented filtering: Geophysics, **68**, 1286–1293.

Nash, S. G., and A. Sofer, 1996, Preconditioning reduced matrices: SIAM J. Matrix Anal. Appl., **17**, 21–34.

Parks, D., 2010, Seismic image flattening as a linear inverse problem: M.S. Thesis, Colorado School of Mines.

Posamentier, H., R. Davies, J. Cartwright, and L. Wood, 2007, Seismic geomorphology - an overview: in: R.J. Davies, H.W. Posamentier, L.J. Wood, J.A. Cartwright (Eds.), Seismic Geomorphology, Geological Society of London Special Publication, 1–14.

Saad, Y., 1996, Iterative methods for sparse linear systems: PWS Publishing Company, Boston.

Stark, T. J., 2005, Generating a seismic Wheeler volume: 75th Ann. Internat. Mtg., Soc. of Expl. Geophys., 782–785.

Vail, P. R., R. G. Todd, and J. B. Sangree, 1977, Seismic stratigraphy and global changes of sea level: Part 5. chronostratigraphic significance of seismic reflections: Section 2. application of seismic reflection configuration to stratigraphic interpretation: M 26: Seismic Stratigraphy-Applications to Hydrocarbon Exploration, AAPG Memoirs, 99–116.

van Vliet, L. J., and P. W. Verbeek, 1995, Estimators for orientation and anisotropy in digitized images: ASCI95, Proc. First Annual Conference of the Advanced School for Computing and Imaging (Heijen, NL, May 16-18), ASCI, 442–450.

Wu, X., and G. Zhong, 2012a, Generating a relative geologic time volume by 3D graph-cut phase unwrapping method with horizon and unconformity constraints: Geophysics, **77**, 21–34.

———, 2012b, A method for generating a seismic Wheeler volume via a relative geologic time volume: 82nd Ann. Internat. Mtg, Soc. of Expl. Geophys., 1–5.

Zeng, H., M. M. Backus, K. T. Barrow, and N. Tyler, 1998a, Stratal slicing; Part 1, Realistic 3-D seismic model: Geophysics, **63**, 502–513.

Zeng, H., S. C. Henry, and J. P. Riola, 1998b, Strata slicing; Part ii, Real 3-D seismic data: Geophysics, **63**, 514–522.